AGU PUBLICATIONS

JGR

Journal of Geophysical Research: Atmospheres

RESEARCH ARTICLE
10.1002/2016JD025001

Key Points:
- Using a global climate model (HadGEM2-CCS), we test the sensitivity of volcanic aerosol dispersion to various SO2 emission scenarios
- Volcanic eruptions initiated on consecutive days could result in vastly different spatial distributions of aerosols
- A 10 day Pinatubo-like eruption is unable to produce the aerosol self-lofting needed to move the aerosol into the southern hemisphere

Supporting Information:
- Supporting Information S1
- Movie S1

Correspondence to:
A. C. Jones,
anthony.jones@metoffice.gov.uk

Citation:
Jones, A. C., J. M. Haywood, A. Jones, and V. Aquila (2016), Sensitivity of volcanic aerosol dispersion to meteorological conditions: A Pinatubo case study, *J. Geophys. Res. Atmos.*, *121*, 6892–6908, doi:10.1002/2016JD025001.

Received 29 FEB 2016
Accepted 2 JUN 2016
Accepted article online 6 JUN 2016
Published online 24 JUN 2016

Sensitivity of volcanic aerosol dispersion to meteorological conditions: A Pinatubo case study

Anthony C. Jones[1,2], James M. Haywood[1,2], Andy Jones[2], and Valentina Aquila[3,4]

[1]College of Engineering, Mathematics, and Physical Sciences, University of Exeter, Exeter, UK, [2]Met Office Hadley Centre, Exeter, UK, [3]Department of Earth and Planetary Sciences, GESTAR/Johns Hopkins University, Baltimore, Maryland, USA, [4]NASA Goddard Space Flight Center, Greenbelt, Maryland, USA

Abstract Using a global climate model (Hadley Centre Global Environment Model version 2-Carbon Cycle Stratosphere) with a well-resolved stratosphere, we test the sensitivity of volcanic aerosol plume dispersion to meteorological conditions by simulating 1 day Mount Pinatubo-like eruptions on 10 consecutive days. The dispersion of the volcanic aerosol is found to be highly sensitive to the ambient meteorology for low-altitude eruptions (16–18 km), with this variability related to anomalous anticyclonic activity along the subtropical jet, which affects the permeability of the tropical pipe and controls the amount of aerosol that is retained by the tropical reservoir. Conversely, a high-altitude eruption scenario (19–29 km) exhibits low meteorological variability. Overcoming day-to-day meteorological variability by spreading the emission over 10 days is shown to produce insufficient radiative heating to loft the aerosol into the stratospheric tropical aerosol reservoir for the low eruption scenario. This results in limited penetration of aerosol into the southern hemisphere (SH) in contrast to the SH transport observed after the Pinatubo eruption. Our results have direct implications for the accurate simulation of past/future volcanic eruptions and volcanically forced climate changes, such as Intertropical Convergence Zone displacement.

1. Introduction

After weeks of precursory activity, Mount Pinatubo in the Philippines (15°N, 121°E) erupted on 15 June 1991 in a volcanic episode that lasted ~9 h starting at 14:00 (local time), although 90% of the total magmatic injecta was emitted in an intense phase that last ~3 h [*Holasek et al*., 1996; *Guo et al*., 2004; *Self et al*., 2004]. The Pinatubo eruption was significant for multiple reasons. It was the first major volcanic eruption to be comprehensively documented by satellite instruments, lidars, and airborne aerosol counters [*McCormick et al*., 1995]; it likely produced the greatest volume of volcanic material injected into the atmosphere of any twentieth century eruption [*Bluth et al*., 1992; *Robock*, 2000]; and it had a broad climatic influence that would prove a vital validation tool for the burgeoning global climate model (GCM) development community. The Pinatubo eruption induced a global mean lower tropospheric cooling of 0.3°C (averaged over the subsequent 4 years) [*Soden et al*., 2002], enhanced ozone reaction catalysis for 1–2 years [*Hofmann et al*., 1992; *McCormick et al*., 1995], disrupted the hydrological cycle [*Spencer et al*., 1998; *Trenberth and Dai*, 2007], induced a tropical stratospheric warming [*Labitzke and McCormick*, 1992], and instigated a wealth of other climatic perturbations [e.g., *McCormick et al*., 1995; *Russell et al*., 1996; *Robock*, 2000].

The primary driver of these climatic impacts was the volcanic aerosol that resided in the stratosphere for multiple years and influenced both the incoming shortwave (SW) radiation and outgoing longwave (LW) radiation [*Stenchikov et al*., 1998]. This aerosol plume was primarily composed of sulfate (SO_4) in the form of liquid sulfuric acid (H_2SO_4) droplets (60–80% by mass) in aqueous solution, formed from the oxidation of gaseous sulfur dioxide (SO_2), which was oxidized to SO_4 with an *e*-folding time of ~35 days [*Bluth et al*., 1992]. Heavier constituents of the initial plume such as ash were removed from the atmosphere within weeks and therefore provided a short-term, localized climatic forcing [*Russell et al*., 1996; *Niemeier et al*., 2009]. Early observations from the Total Ozone Mapping Spectrometer suggested that Pinatubo emitted ~20 teragrams (Tg) of SO_2 [*Bluth et al*., 1992], although a later, revised estimate suggested 14–23 Tg [*Guo et al*., 2004]. Recent Pinatubo simulations with models that incorporate aerosol microphysics suggest that an SO_2 emission of nearer 14 Tg produces better agreement with observations [*Sheng et al*., 2015].

The evolution of the aerosol cloud was observed by the advanced very high resolution radiometer (AVHRR) and Stratospheric Aerosol and Gas Experiment II (SAGE-II) satellite-borne instruments [*Stowe et al*., 1992;

McCormick and Veiga, 1992]. After the eruption, the aerosol plume was rapidly transported westward via zonal stratospheric winds and encircled the Earth within 22 days [*Bluth et al*., 1992]. Additionally, the aerosol cloud was initially advected both northward and southward, crossing the equator within 1 week [*Young et al*., 1994]. Subsequent meridional transport was impeded by the "leaky tropical pipe"—a sharp latitudinal potential vorticity gradient in the subtropical stratosphere—and later by the strong polar night jet in the southern hemisphere (SH) [*Boville et al*., 1991]. For the first couple of months after the eruption, the aerosol cloud was primarily confined to the tropical stratosphere (20°S–30°N), within altitudes of 20–30 km [*McCormick et al*., 1995]. The contemporaneous descending easterly shear phase of the quasi-biennial oscillation (QBO), coupled with a strong lower stratospheric meridional wind gradient in the subtropics, contributed to the initial confinement of the aerosol to the tropics [*Trepte and Hitchman*, 1992; *Trepte et al*., 1993; *Choi et al*., 1998]. By July 1991, aerosol in the lower stratosphere (~16 km/100 hPa altitude) had been transported to high northern hemisphere (NH) latitudes (>50°N), primarily through advection by a tropospheric quasi-stationary anticyclone over Asia [*McCormick et al*., 1995; *Trepte et al*., 1993; *Timmreck et al*., 1999b]. Additionally, aerosol was later transported to the NH at higher altitudes (~25 km/ 30 hPa altitude) in the months following the shift from summer to winter stratospheric dynamics in October 1991 [*Trepte et al*., 1993]. Significant aerosol transport into the SH occurred during September 1991 in the high-altitude regime (~22 km/40 hPa altitude), primarily as the result of transient subtropical anticyclones [*Trepte et al*., 1993]. The global sulfate cloud decayed exponentially with an e-folding time of ~1–2 years [*Kirchner et al*., 1999; *Driscoll et al*., 2012].

Various GCMs have been used to simulate the dispersal of the Pinatubo aerosol cloud. Early experiments treated the aerosol as a passive tracer, which disregards the radiative feedback of the aerosol [*Boville et al*., 1991; *Pudykiewicz and Dastoor*, 1995; *Timmreck et al*., 1999b]. *Young et al*. [1994] combined a 3-D circulation model with an aerosol transport/radiation code to show the importance of including the radiative feedback on the resultant dispersion of the aerosol. *Timmreck et al*. [1999a] showed that the stratospheric dynamical adjustments from aerosol-induced radiative heating could induce a strengthening of the polar vortex, in agreement with observations from 1991/1992 [e.g., *Robock and Mao*, 1995]. However, the simulated tropical aerosol reservoir in *Timmreck et al*. [1999a] was short-lived compared with observations, which the authors attributed to the absence of a QBO in their GCM. The QBO is a periodic oscillation of the equatorial, stratospheric zonal mean, zonal wind direction at ~40 hPa altitude [*Baldwin et al*., 2001]. Pinatubo simulations with GCMs that do not include a QBO have generally exhibited a short-lived tropical aerosol reservoir [*Oman et al*., 2006; *Niemeier et al*., 2009; *Toohey et al*., 2011]. *Niemeier et al*. [2009] coupled an aerosol microphysics module with a GCM to show that radiative heating induced by the short-lived ash ejected by Pinatubo could alter the initial trajectory of the sulfate plume. *Toohey et al*. [2011] showed that the Pinatubo aerosol optical depth (AOD) evolution is sensitive to the season of eruption (particularly in the NH), which they attributed to the state of the Brewer-Dobson circulation (BDC) in the stratosphere. *Aquila et al*. [2012] (hereafter, AQ12) simulated Pinatubo using the Goddard Earth Observing System version 5 GCM, which included a single-moment sulfate-transport scheme and radiatively interactive aerosol, but no QBO representation. They injected 20 Tg [SO_2] at the comparatively low altitudes of 16–18 km over a single day in eight consecutive "15 Junes" and with perpetual year 2000 conditions. The low-altitude specification was selected because sensitivity tests with high-altitude eruptions (16–25, 17–27, 20–27, and 20–30 km) had elevated the aerosol to altitudes that exceeded observations [e.g., *McCormick and Veiga*, 1992]. Their ensemble mean 550 nm AOD evolution (Figure 2 of AQ12) compared well to AVHRR and SAGE II observations. *English et al*. [2013] coupled a 3-D sectional aerosol model to a GCM to study the linearity of atmospheric aerosol burdens to increasing levels of SO_2 emissions, finding a nonlinear relationship due to enhanced aerosol growth and sedimentation. To compensate for the omission of radiatively interactive aerosol and a QBO, *English et al*. [2013] injected over a wide area (2°S–14°N, 95°E–115°E) and vertical span (15–29 km altitude), a technique also utilized by *Timmreck et al*. [1999a], *Weisenstein et al*. [2007], and *Dhomse et al*. [2014]. This "wide-injection" method sidesteps the necessary radiatively induced dynamical changes required to transport the aerosol southward and upward (AQ12). *Dhomse et al*. [2014] used a detailed aerosol microphysics module coupled to a GCM with an internally generated QBO to show that a simulated 10 Tg [SO_2] Pinatubo-like eruption produced aerosol size distributions that matched observations better than the ubiquitously utilized 20 Tg [SO_2] emission rate. *Mills et al*. [2016] also found that a 10 Tg [SO_2] injection produced the best fit to Pinatubo observations, while *Sheng et al*. [2015] found that 14 Tg [SO_2] produced the best fit. However, climate models are imperfect tools for inferring the quantity of SO_2 emitted by a volcanic eruption due to scenario-based uncertainties such as the altitude and composition of the volcanic plume, model-specific

limitations such as coarse spatiotemporal resolutions and parameterized processes, missing processes such as the co-injection of volcanic ash, and internal variability such as meteorological conditions.

A previously unexplored aspect of the Pinatubo eruption is the role of meteorology in the evolution of the aerosol plume, although the ensemble standard deviations in Figures 1 and 3 of AQ12 and Figures 5d–5f of *Toohey et al*. [2011] suggest a high meteorological sensitivity in previous simulations. The spread of the aerosol plume has implications for the climatic impacts of volcanic eruptions. For instance, *Haywood et al*. [2013] showed that enhancement of the stratospheric sulfate burden in a single hemisphere could alter the position of the Intertropical Convergence Zone (ITCZ) and associated monsoon precipitation. The aim of this investigation is to explicitly assess the sensitivity of the Pinatubo aerosol dispersion to the ambient meteorology. Additionally, we compare the aerosol dispersion from a 10 day eruption to the ensemble mean of ten 1 day eruptions, which represent two intuitive methods of overcoming meteorological variability whilst simulating a volcanic eruption. In section 2 we describe the GCM (Hadley Centre Global Environment Model version 2-Carbon Cycle Stratosphere (HadGEM2-CCS)) used for this investigation and the Pinatubo simulation suite. In section 3.1 we compare the global mean sulfate optical depth anomalies for the Pinatubo simulations to observations. In section 3.2 we compare the aerosol dispersion for the ensemble mean of the 1 day eruptions with the 10 day eruption. In section 3.3 we compare the aerosol dispersion for individual 1 day eruption simulations to assess the importance of meteorology. We discuss the significance of our results in the context of potential climatic impacts of future volcanic eruptions and future GCM Pinatubo simulations in section 4.

2. Methods

2.1. Model

We use the HadGEM2-CCS GCM in atmosphere-only mode with prescribed climatological sea surface temperatures and sea ice fields. HadGEM2-CCS is the high-top configuration of the HadGEM2 family of models, with the atmospheric submodel comprising 60 vertical levels extending to approximately 84 km (~0.01 hPa) altitude and with a horizontal resolution of 1.25° latitude by 1.875° by longitude [*Martin et al*., 2011]. We use perpetual Pre-Industrial Control (piControl) baseline conditions derived from Coupled Model Intercomparison Project Phase 5 (CMIP5) specifications [*Jones et al*., 2011; *Taylor et al*., 2012]. This includes prescribed ozone fields following *Cionni et al*. [2011] and fixed atmospheric concentrations of carbon dioxide (CO_2), methane (CH_4), and nitrous oxide (N_2O). Except for the process of methane oxidation, HadGEM2-CCS does not include stratospheric chemistry but does include a well-resolved stratosphere capable of internally generating a realistic QBO [*Hardiman et al*., 2012; *Watson and Gray*, 2014]. The internal QBO is forced by parameterized orographic and nonorographic gravity wave drag schemes [*Martin et al*., 2011]. HadGEM2-CCS has been used for assessing the impacts of climate change on the stratospheric polar vortex strength [*Mitchell et al*., 2012], the climatic impacts of stratospheric geoengineering schemes [*Jackson et al*., 2015; *Jones et al*., 2016], and the influence of solar variability on surface climate [*Gray et al*., 2013]. Additionally, *Haywood et al*. [2010] simulated the 2008 Sarychev volcanic eruption with an atmosphere-only configuration of HadGEM2-CCS (as used here). *Haywood et al*. [2010] found that the simulated SO_2 dispersion closely resembled Infrared Atmospheric Sounding Interferometer observations and the SO_4 showed reasonable agreement with that derived from the Optical Spectrograph and Infrared Imager System limb-sounding instrument.

HadGEM2-CCS includes the Coupled Large-scale Aerosol Simulator for Studies in Climate (CLASSIC) aerosol module, which is described in detail by *Martin et al*. [2006], *Bellouin et al*. [2011], and references therein. The sulfur cycle includes the oxidation of gaseous SO_2 and dimethyl sulfide (DMS) to form sulfate aerosol, which is represented by two optically active modes (Aitken and accumulation) and a dissolved/in-cloud mode. The sulfate scheme represents the processes of nucleation, evaporation, coagulation, diffusion, and hygroscopic growth [*Bellouin et al*., 2011]. Aerosol is removed from the atmosphere via wet and dry deposition (important in the troposphere) and sedimentation (important in the stratosphere) with sedimentation rates calculated by applying Stokes' law [*Jones et al*., 2016]. DMS emissions and atmospheric oxidants (such as the $OH^{\cdot}$ free radical) are prescribed for the duration of the simulations, according to piControl conditions. CLASSIC's sulfate accumulation mode is modified for this investigation in order to reflect the larger aerosols observed after volcanic eruptions [*Russell et al*., 1996]. The modified accumulation mode is represented by a lognormal distribution with geometric mean radius of $r_m = 0.376\,\mu m$ and standard deviation of $\sigma = 1.25$

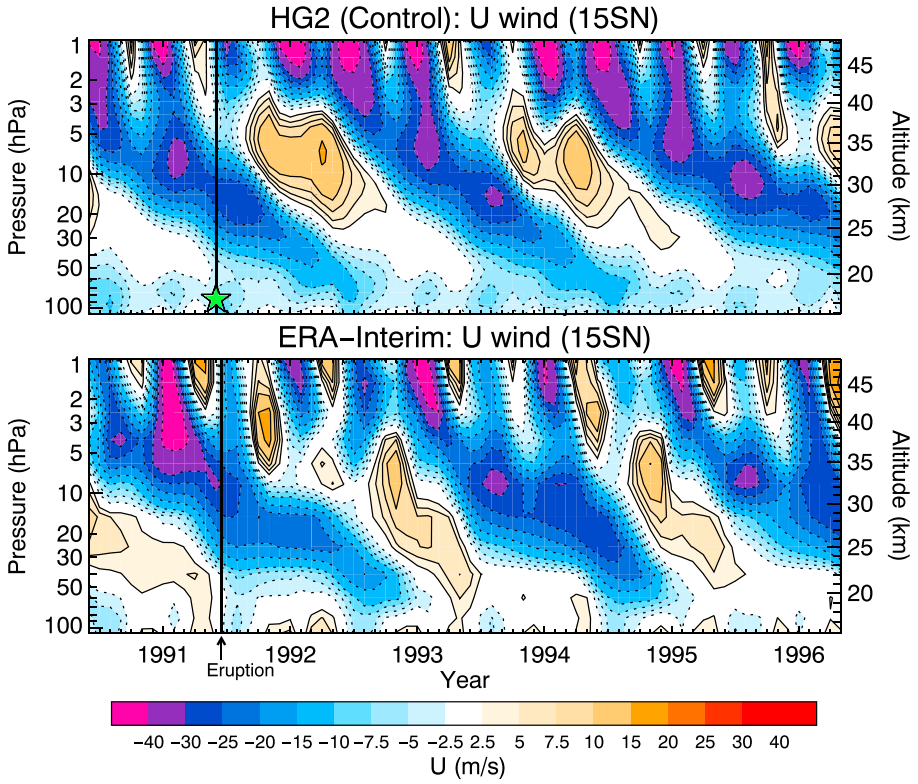

Figure 1. Zonal mean, zonal wind during the Pinatubo-eruption era for (a) the HadGEM2-CCS control simulation and (b) ERA-interim reanalysis data [*Dee et al.*, 2011].

[*Rasch et al.*, 2008], with the corresponding optical properties shown in Figure 1a of *Jones et al.* [2016]. This size distribution is applied throughout the atmosphere, which will have some influence on the tropospheric sulphur cycle and the associated aerosol-radiation and aerosol-cloud interactions. By prescribing a fixed radius, the model is unable to accurately represent the physical and optical properties of the evolving aerosol size distribution within the aerosol plume [*Dhomse et al.*, 2014]. The dry-mode effective radius of this distribution (0.42 μm) is similar to the peak effective radius between 1 to 200 hPa from the Pinatubo simulations of *English et al.* [2013]. The choice of size distribution affects the sedimentation velocity of the aerosol particles. For the size distribution used here, *Jones et al.* [2016] found an average sedimentation rate between 18 and 26 km altitude of 23 m/d and between 26 and 30 km of 52 m/d. The model's radiation scheme [*Edwards and Slingo*, 1996] is coupled to the dynamics, allowing for radiatively induced aerosol self-lofting [*Young et al.*, 1994].

2.2. Pinatubo Simulation Design

A 40 year piControl simulation was initially conducted, from which we selected a model year in which the simulated QBO in June resembled the Pinatubo-concurrent QBO conditions. Specifically, Mount Pinatubo erupted in June 1991, at which time the QBO had entered an easterly phase 2 months previously [*Hansen et al.*, 1992]. *Trepte et al.* [1993] showed that the transport of aerosol after large tropical volcanic eruptions is highly sensitive to the contemporaneous QBO phase. A time series of our simulated QBO compared with the ERA-Interim re-analyses for the Pinatubo period is shown in Figure 1. Our Pinatubo simulations were initiated from June in the selected model year (time/altitude indicated in Figure 1 by a green star). We performed a single control simulation with no additional SO_2 emission, a single simulation with a continuous 10 day eruption (*10D*), in which SO_2 is emitted evenly between 1 and 10 June; 10 simulations with 1 day eruptions (*1D*), in which SO_2 is emitted evenly over a 24 h period on 1, …, 10 June; and 10 simulations with 3 h eruptions (*3H*), in which SO_2 is emitted evenly over a 3 h period from 14:00 to 17:00 on 1, …, 10 June. The *1D* scenario was chosen following the simulation design of AQ12. However, as 90% of the total mass injected by Pinatubo on 15 June occurred during an ~3 h phase from 14:00 to 17:00 [*Holasek et al.*, 1996; *Self et al.*, 2004], we also examine any differences that may occur when representing Pinatubo emissions with a 3 h

Table 1. List of Performed Experiments[a]

Name	Injection Height (km)	Duration of Eruption	Total SO_2 Emitted (Tg)	Ensemble Members	Ensemble Mean Name
Control	N/A	N/A	N/A	1	N/A
10D_HIGH	19–29	10 days	14	1	N/A
1D_HIGH	19–29	1 day	14	10	1D_HIGH_AV
10D_LOW	16–18	10 days	20	1	N/A
1D_LOW	16–18	1 day	20	10	1D_LOW_AV
1D_LOW + CH	16–18 (P)	1 day (P)	20 (P)	2	N/A
	11–16 (CH)	8 h (CH)	3.3 (CH)		
3H_LOW	16–18	3 h	20	10	3H_LOW_AV

[a]For the 1D_LOW + CH simulations, "P" refers to Pinatubo and "CH" refers to Cerro Hudson.

eruption. For each of the Pinatubo simulations, SO_2 is injected into a single horizontal grid cell at (15°N, 120°E). We test two Pinatubo-like eruption scenarios that have been used in the literature. First, we adopt a similar eruption design to AQ12, in which 20 Tg [SO_2] is injected evenly between 16 and 18 km (100–70 hPa) altitude (two vertical model levels), and denote these experiments *LOW*. Second, we adopt a similar eruption design to *Dhomse et al.* [2014] and inject 14 Tg [SO_2] evenly between 19 and 29 km (65–15 hPa) altitude (nine vertical model levels) and denote these experiments *HIGH*. The *HIGH* scenario differs slightly from *Dhomse et al.* [2014], who injected 10 and 20 Tg [SO_2] between 19 and 27 km altitude. *Sheng et al.* [2015] found that 14 Tg [SO_2] injection at high altitudes produces a close match to observations. The experiments are listed in Table 1. The results of the 1 day *LOW* eruption ensemble mean (*1D_LOW_AV*) were also used by *Jones et al.* [2016] for model validation purposes and are plotted in their Figure 2. Although the simulated climatology is "perpetual piControl," we use the equivalent Pinatubo year for plotting/references to facilitate comparison with observations.

3. Results

3.1. Global-Mean Sulfate Optical Depth

The primary climatological field assessed in this research is the 550 nm sulfate aerosol optical depth (AOD), which was diagnosed in the aftermath of the Pinatubo eruption by the AVHRR and SAGE-II satellite-borne instruments, albeit at slightly different wavelengths of 630 nm and 525 nm, respectively [*Stowe et al.*, 1992; *McCormick and Veiga*, 1992]. Figure 2 shows the monthly mean 550 nm AOD anomaly, averaged between 75°S and 75°N, for the HadGEM2-CCS (HG2) *1D* and *10D* simulations and the AVHRR and SAGE-II observations. AVHRR data are only collected over the cloud-free global oceans and are based on the updated data of *Zhao et al.* [2013] (available from https://www.ncdc.noaa.gov/cdr/atmospheric/avhrr-aerosol-optical-thickness). For SAGE II, we use the updated gap-filled aerosol-extinction climatology developed for Chemistry-Climate Model Initiative simulations based on the SAGE_4λ method [*Arfeuille et al.*, 2013]. The SAGE_4λ data set uses observations from the Cryogenic Limb Array Etalon Spectrometer (CLAES) and Halogen Occultation Experiment instruments when SAGE II data are unavailable (*L. Thomason*, personal communication, 2016). To retrieve SAGE_4λ AODs, we integrate aerosol extinctions above the tropopause height, where the tropopause is derived from our HG2 simulations as in *Mills et al.* [2016]. For AVHRR, we subtract the monthly mean AODs from the year 1990 to calculate anomalies, which was the approach used by AQ12 and *Mills et al.* [2016]. For

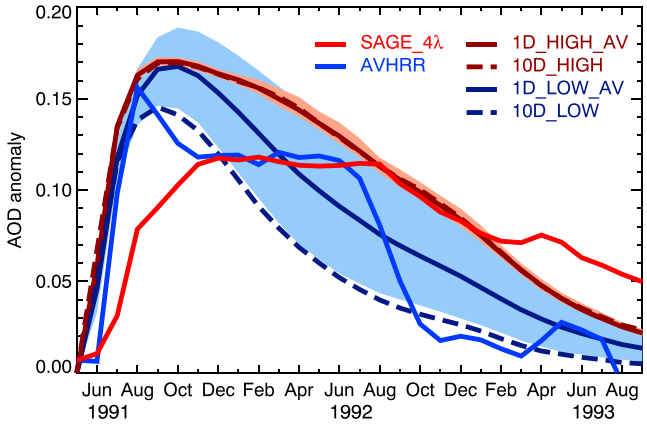

Figure 2. 75°S–75°N mean sulfate 550 nm AOD anomaly for the HadGEM2-CCS simulations and SAGE II (red) and AVHHR (blue) observations. The blue shaded area shows the range of the 1D_LOW ensemble; the orange shaded area shows the range of the 1D_HIGH ensemble.

HG2, we subtract the parallel AOD of the *CONTROL* simulation to calculate anomalies. The blue and orange shaded areas in Figure 2 show the range for the *1D_LOW* and *1D_HIGH* experiments, respectively. From Figure 2, it is clear that both the *1D_LOW_AV* and the *1D_HIGH_AV* AODs are initially in close agreement with the AVHRR values, with a peak in October 1991 of ~0.17 and exponential decline thereafter. As discussed by multiple authors, SAGE II was unable to capture the peak AOD for the first few months after Pinatubo due to saturation at AODs >0.15 [*Russell et al*., 1996]. Despite the integration of CLAES data with SAGE II data to overcome this saturation issue (*L. Thomason*, personal communication, 2016), the updated SAGE_4λ data set is still unable to capture the peak aerosol extinctions in the immediate aftermath of the eruption. However, the greater coverage of the SAGE II observations and the instrument's ability to detect lower AODs than AVHRR (<0.02) [*Stowe et al*., 1992] make it useful for later AOD values. In particular, from January 1992 the aerosol plume had diminished sufficiently for SAGE_4λ and AVHRR AODs to be similar on the global mean scale (Figure 2). A few aspects of the HG2 AODs in Figure 2 are salient: (1) *10D_LOW* is significantly less than *1D_LOW_AV* and peaks in September 1991 at ~0.145 rather than October 1991 with a peak of ~0.17; (2) the *1D_LOW* ensemble spread is broad, for instance, the maximum AOD in April 1992 is ~0.15 compared a minimum of ~0.065; and (3) the *1D_HIGH* ensemble spread is small, suggesting that the aerosol dispersion after a high-altitude SO_2 emission would be less sensitive to the ambient meteorology.

Figure S1 in the supporting information compares the global 550 nm sulfate AOD anomaly for the *3H_LOW* and *1D_LOW* simulations. It is clear that the 3 h and 1 day eruptions produce very similar AODs, both in terms of ensemble mean and the ensemble range. This result could be an artefact of our model; a better representation of the aerosol microphysics within the evolving aerosol plume might yield greater differences between the 3 h and 24 h eruption scenarios than shown here due to differing feedback between the aerosol and the meteorology. However, for the basis of this investigation and due to the similarity between the AOD evolutions, we present results from the aerosol dispersion from the *1D_LOW* simulations instead of the *3H_LOW* simulations for consistency with AQ12.

3.2. 10 day Eruption Against 1 Day Eruption Ensemble Mean

Figure 3 shows the time series of zonal mean AOD anomaly for the *10D* experiments and the ensemble means of the *1D* experiments and for SAGE_4λ and AVHRR observations. For the HG2 experiments, we use the zonal mean AOD over oceans from May 1991 to December 1991 for best comparison with AVHRR. The R^2 values given in Figure 3 for the HG2 AOD fields are calculated with respect to AVHRR from July to December 1991 and SAGE_4λ thereafter (Figure S2 shows the composite AVHRR/ SAGE_4λ field). R^2, the coefficient of determination, describes the proportion of the variance in the observations that can be explained by the model (ranging from 0 to 1, with higher values indicating better agreement) [*Legates and McCabe*, 1999]. While *1D_LOW_AV* captures the transport of aerosol into the SH as observed by SAGE II and AVHRR, the *10D_LOW* volcanic aerosol is entirely confined to the NH. It is clear from the R^2 values that *1D_LOW_AV* describes slightly more of the variability in the observations than *1D_HIGH_AV* (R^2 of 0.31 compared to 0.25) and that *1D_LOW_AV* is a much better fit to the observations than *10D_LOW*. The difference in AOD in the SH between *1D_LOW_AV* and the observations is partially attributable to the Cerro Hudson eruption in August 1991 at (46°S, 73°W), which injected 3.3 Tg [SO_2] into the stratosphere [*Deshler and Anderson-Sprecher*, 2006] and is not represented in these simulations. The Cerro Hudson aerosol was able to penetrate deep into the SH immediately (because of the volcano's location), while the Pinatubo aerosol was contemporaneously confined to the tropical vortex [*McCormick et al*., 1995; *Legrand and Wagenbach*, 1999]. We chose not to represent the Cerro Hudson eruption in these simulations as the primary purpose is to investigate the influence of meteorological variability on the evolution of the plume from Pinatubo from HG2. By omitting representation of Cerro Hudson, a "perfect" Pinatubo simulation would not produce $R^2=1$, because the AVHRR/ SAGE_4λ observations also include the Cerro Hudson aerosol. Therefore, R^2 as used in Figure 3 only provides an approximate measure of "goodness of fit" between the model and observations.

Figure 4 shows the equatorial SO_2 concentration anomaly plotted against altitude in September 1991 for *10D_HIGH*, *1D_HIGH_AV*, *10D_LOW*, and *1D_LOW_AV*. Observations from the Microwave Limb Sounder (MLS) [*Read et al*., 1993] are indicated by the black circles in Figure 4. It is clear that *1D_LOW_AV* best captures the peak of the SO_2 plume as observed by the MLS at ~22 hPa altitude. However, *1D_LOW_AV* overestimates the SO_2 concentrations at ~50 hPa compared to the MLS observations, which could be due to SO_2 removal processes that are not represented in the model such as deposition on ash or ice, or it could be due to the

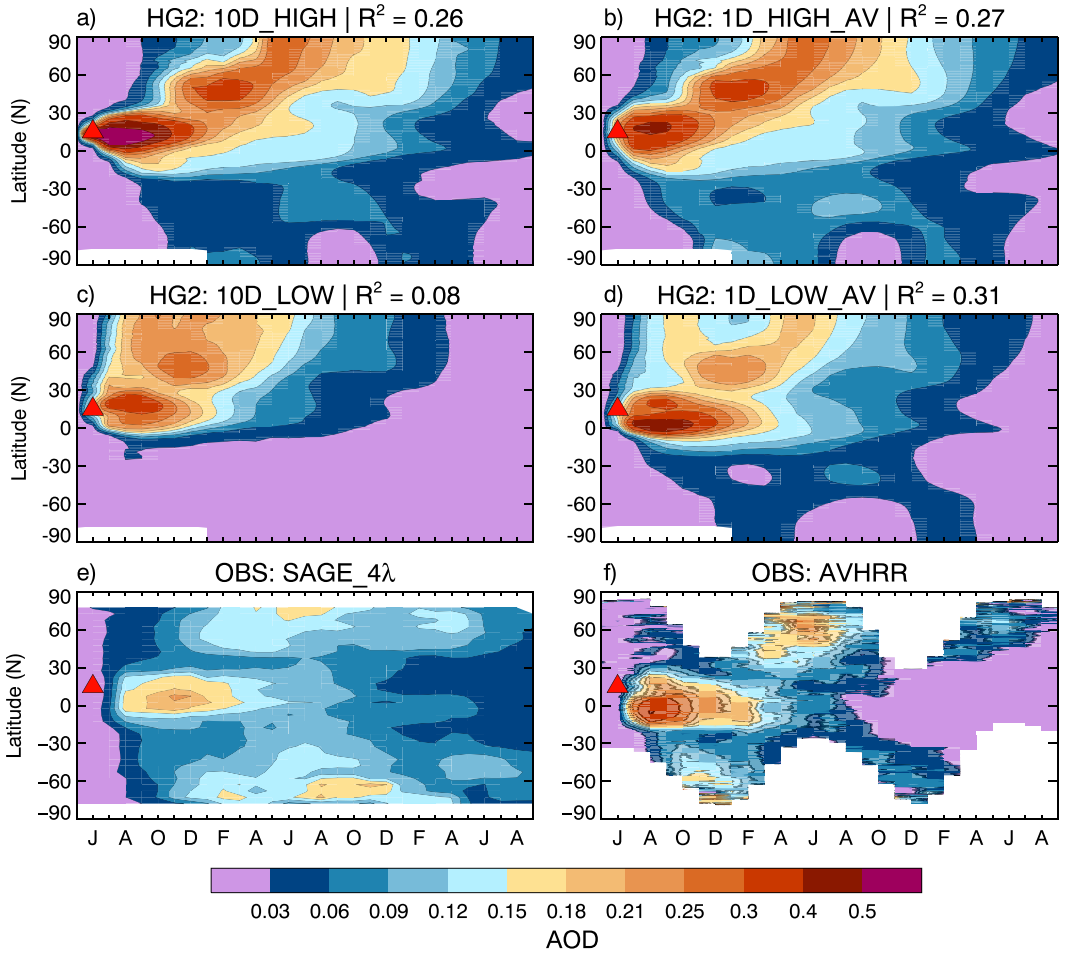

Figure 3. Latitude versus time plot of monthly/zonal mean sulfate 550 nm AOD anomaly for (a) 10D_HIGH, (b) 1D_HIGH_AV, (c) 10D_LOW, (d) 1D_LOW_AV, (e) SAGE II, and (f) AVHRR. The red triangles indicate the Pinatubo eruption.

fixed aerosol radius used here. The 14 Tg [SO_2] *HIGH* simulations fail to capture the peak of the SO_2 plume; however, the *HIGH* simulations do provide a better fit to the MLS observations at ~10 hPa than the *LOW* simulations. This suggests that our simulations of Pinatubo with HG2 are better represented by *LOW* than *HIGH* injection profiles although we recognize that the best representation of injection profile would be somewhat higher than *LOW* but considerably lower than *HIGH*. For the rest of this analysis, we focus on the *LOW* experiments as the *1D_LOW* ensemble mean provides the best fit to the observations such that that while *1D_LOW_AV* has a similar global mean AOD to *1D_HIGH_AV* (Figure 2), it has a better R^2 in the horizontal (Figure 3) and a better vertical SO_2 distribution when compared to observations (Figure 4).

From Figure 4, the *10D_LOW* SO_2 concentrations are much smaller than the Microwave Limb Sounder (MLS) measurements reported by *Read et al.* [1993] and peak at 40 hPa altitude rather than the ~25 hPa altitude from observations. Conversely, the *1D_LOW_AV* and most of the *1D_LOW* ensemble's SO_2 concentrations are similar to observations (e.g., ~14 ppbv at 22 hPa). Figure 5 shows the atmospheric zonal mean SO_4 mass mixing ratio anomalies for *1D_LOW_AV* and *10D_LOW* for July, September, November, and December 1991. From Figure 5, the sulfate reservoir in the tropics in July is at a higher altitude for *1D_LOW_AV* than for *10D_LOW* and closer to the equator; for instance, the peak mass mixing ratio anomaly (indicated by the dashed lines in Figure 5) in July for *1D_LOW_AV* is at 34 hPa, 4°N and for *10D_LOW* is at 41 hPa, 19°N. *Trepte and Hitchman* [1992] showed that aerosol in the lower tropical stratosphere (>40 hPa altitude) is rapidly transported toward high latitudes, while aerosol at higher altitudes (40–10 hPa altitude) is confined to the tropical pipe. By July, 3 Tg [S] of combined SO_2 and SO_4 has been transported to middle/high NH altitudes (>30°N) in *10D*, compared to 1.9 Tg [S] in *1D_LOW_AV* (Figure S3). The sulfate in the tropical reservoir in

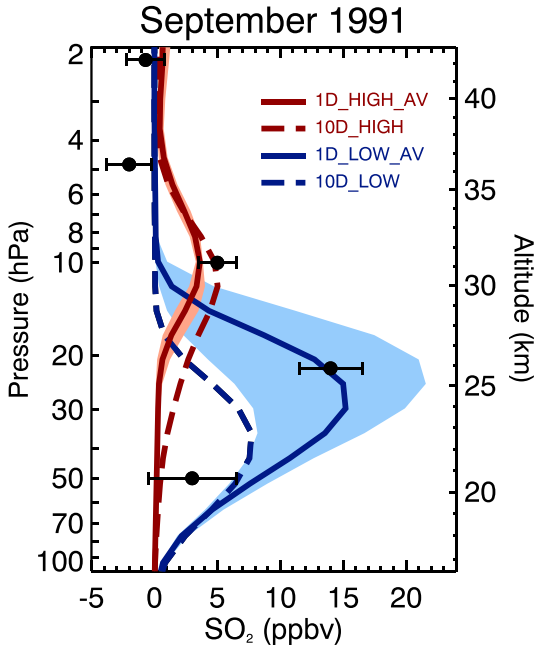

Figure 4. Equatorial (10°S–10°N) mean SO_2 concentration anomaly in September 1991 for 1D_HIGH_AV, 10D_HIGH, 1D_LOW_AV, and 10D_LOW. The black circles indicate Microwave Limb Sounder (MLS) observations as reported in *Read et al.* [1993] with corresponding horizontal lines indicating the standard error of the observations.

1D_LOW_AV is predominantly transported to the SH in the upper branch of the BDC (~30 hPa altitude) in September (Figure 5f), reaching the South Pole by November (Figure 5g), in line with observations [*Trepte et al.*, 1993]. However, the *10D_LOW* aerosol is only transported to the SH in a lower stratospheric pathway at ~100 hPa altitude (Figure 5d).

To explain the difference in meridional transport between *1D_LOW_AV* and *10D_LOW*, it is necessary to compare the radiative heating perturbations. Figure 6 shows (a) the initial clear-sky heating rate anomaly for the duration of the eruption (i.e., 10 days for *10D_LOW* and 1 day for *1D_LOW_AV*) at the eruption location, (b) the equatorial (5°S–5°N) temperature anomaly in July, and (c) the equatorial vertical velocity anomaly in July. The *1D_LOW* simulations clearly exhibit a greater radiative-heating perturbation than for *10D_LOW* (Figure 6a), which is due to the difference in initial mass loading of SO_2. Although the radiative properties of SO_2 are not represented in this model, the SO_4 plume, which immediately begins to form from oxidation of the volcanic SO_2, is also denser for *1D_LOW* than *10D_LOW*, thus inducing a greater radiative heating perturbation, which is counterbalanced by adiabatic cooling from enhanced vertical motion and by temperature tendencies (e.g., equation (3) in *Holton et al.* [1995]). This is exemplified by the greater equatorial heating (Figure 6b) and vertical velocity perturbation (Figure 6c) in *1D_LOW_AV* than *10D_LOW*. The *1D_LOW* aerosol is therefore "self-lofted" to higher altitudes than the *10D_LOW* aerosol and is concomitantly transported in the upper stratospheric pathway in the SH.

The peak aerosol burden anomaly in the *1D_LOW_AV* experiment is 5.8 Tg [S] (Figure S3), which falls within the observed uncertainty range of 3.7 to 6.7 Tg [S] given by *Dhomse et al.* [2014]. By December 1991, 40% of the 10 Tg [S] volcanic sulfur in *1D_LOW_AV* has been removed from the atmosphere. Figure S4 shows the relative contributions to the total sulfur deposition at the surface from the primary removal processes for the first 7 months after the eruption for *10D_LOW* and *1D_LOW_AV*. It is clear that the wet deposition of dissolved sulfate by large-scale precipitation events contributes the largest deposition of sulfur (~60 %), followed by convective scavenging of accumulation-mode sulfate (~25 %). SO_2 deposition by convective scavenging contributes ~4% of the total sulfur deposition, which decreases over time as SO_2 is oxidized to form sulfate.

3.3. "Day 1" Eruption Against "Day 10" Eruption

Figure 7 shows the zonal mean AOD evolution for the individual *1D_LOW* simulations. The first eight ensemble members show reasonable conformity with AVHRR/SAGE_4λ observations, which is quantitatively corroborated by their similar R^2 values (~0.3–0.5). However, the last two simulations (*1D_LOW_9* and *1D_LOW_10*) exhibit minimal transport of aerosol into the SH, in disagreement with the observations (reflected in R^2 values <0.1). The only difference between the simulations is the meteorology encountered by the aerosol plume. Figure S5 shows the zonal mean AOD evolution from AQ12's eight ensemble members (equivalent to our Figure 7). Despite the fact that the meteorology is independent of that in AQ12, we have obtained very similar results—for instance, the difference between their simulations Pin45act4d and Pin45act3d, with the latter showing a persistent NH aerosol plume, is similar to the difference between our *1D_LOW_1* and *1D_LOW_10*.

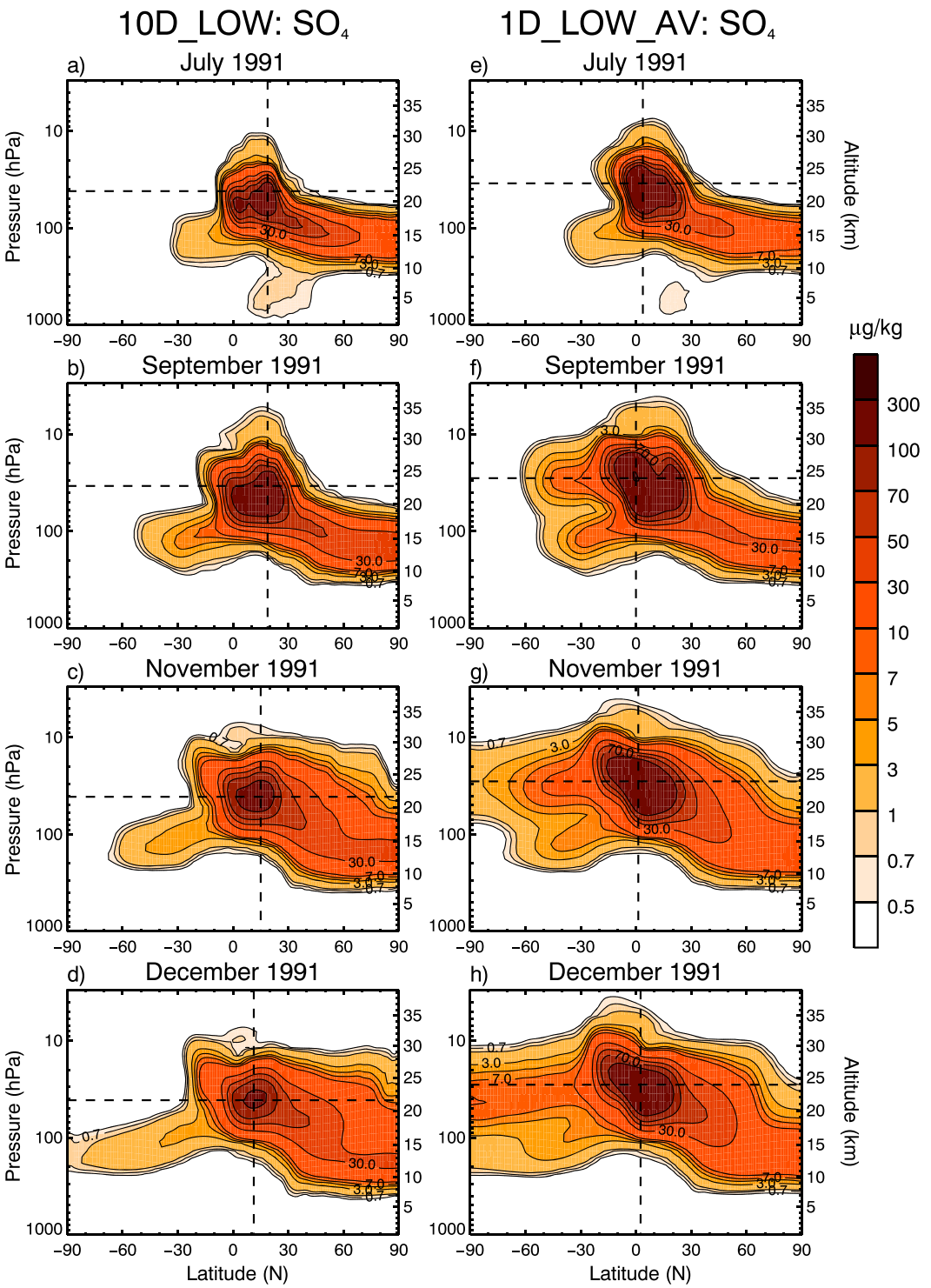

Figure 5. Latitude versus altitude plot of zonal mean sulfate mass concentration anomaly for 10D_LOW and 1D_LOW_AV.

Figure S6 shows the zonal mean AOD evolution for the *3H_LOW* simulations. It is clear that the individual *3H_LOW* simulations are very similar to their counterpart *1D_LOW* simulations; for instance, *1D_LOW_1* and *3H_LOW_1* have R^2 values of 0.50 and 0.48, respectively.

As mentioned in section 3.2, the absence of SH aerosol in the HG2 simulations could partially be attributed to the lack of representation of the Cerro Hudson (CH) eruption, which occurred on 15 August 1991. In order to

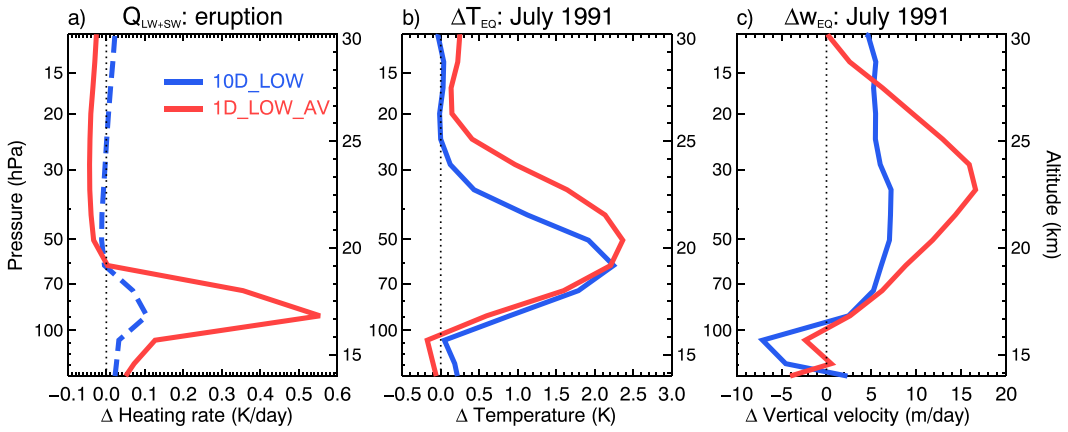

Figure 6. (a) Instantaneous clear-sky heating rate anomaly for the duration of the eruption at 15°N, 120°E, (b) July 1991 zonal mean temperature anomaly averaged between 5°S and 15°N, and (c) July 1991 zonal mean vertical velocity anomaly averaged between 5°S and 15°N.

assess the importance of the CH eruption on SH aerosol in the aftermath of the Pinatubo eruption, we have rerun the 1st and 10th *1D* ensemble members (*1D_LOW_1* and *1D_LOW_10*) with a CH-like eruption included. CH is represented by a 3.3 Tg [SO_2] injection, with SO_2 emitted uniformly between 11 and 16 km altitude from 04:00 to 12:00 on 1 August (2 months after Pinatubo) at 46°S, 73°W [*Schoeberl et al.*, 1993a; *Deshler and Anderson-Sprecher*, 2006]. Figure S7 shows the zonal mean 550 nm AOD evolution for the *1D_LOW_1 + CH* and *1D_LOW_10 + CH* experiments. It is clear that the inclusion of CH in the simulations has not significantly affected the AOD distribution; for instance, the R^2 values for the *1D_LOW_10* and *1D_LOW_10 + CH* experiments are the same (0.09).

Figure 8 shows the total sulfur ($SO_2 + SO_4$) column burden anomaly (g[S]/m^2) for the most disparate *1D_LOW* simulations, *1D_LOW_1* and *1D_LOW_10*, at intervals of 3, 7, 14, and 30 days after the initiation of the eruption (see also Movie S1 in the supporting information). The circled-arrows in Figure 8 show the direction of the

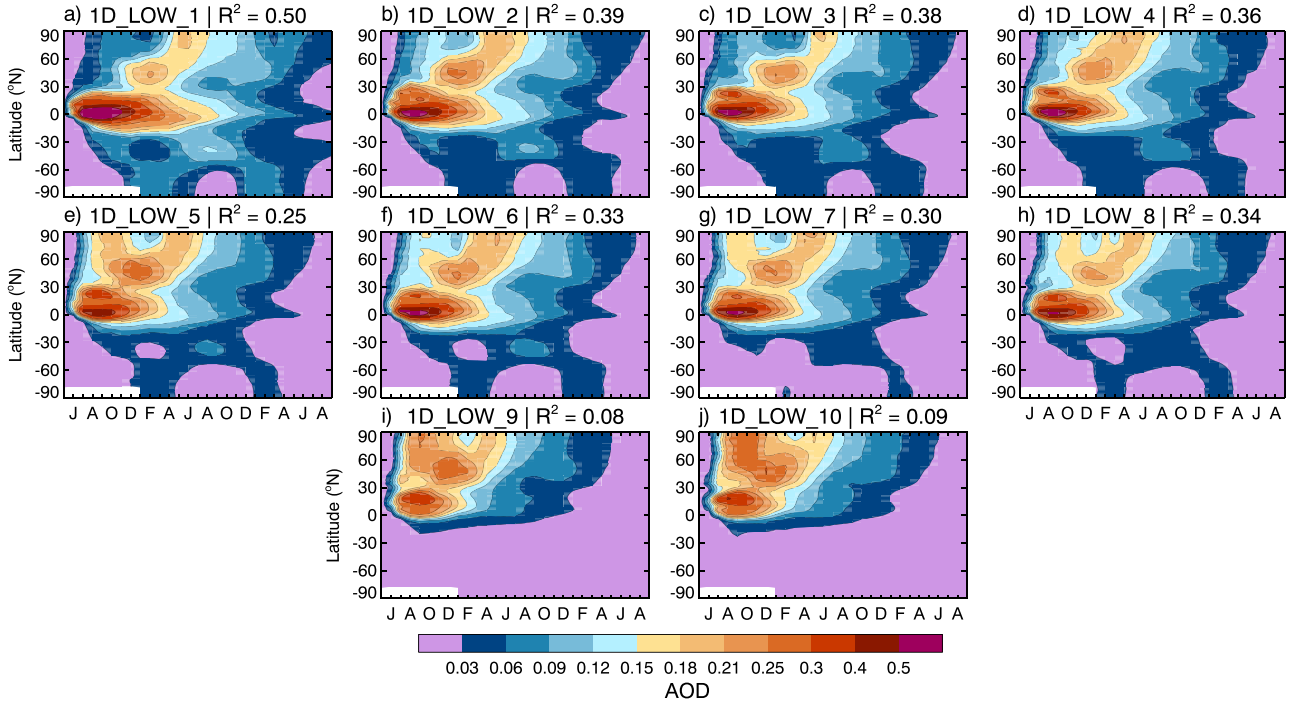

Figure 7. Latitude versus time plot of monthly/zonal mean sulfate 550 nm AOD anomaly for the 1D_LOW ensemble.

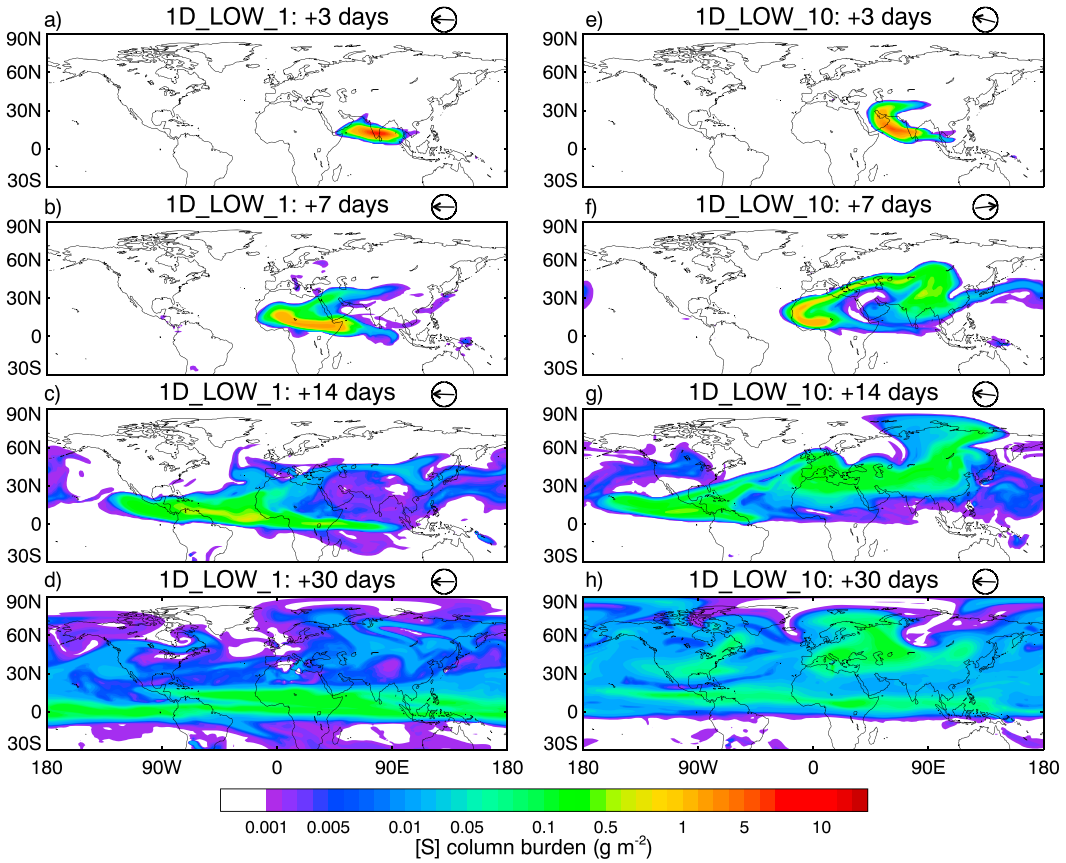

Figure 8. Sulfur ([S]) column burden anomaly for 1D_LOW_1 and 1D_LOW_10 for 3, 7, 14, and 30 days after the eruption. The circled arrows show the direction of the [S]-concentration-anomaly weighted wind vector $[\hat{u}, \hat{v}]$.

[S]-concentration-anomaly weighted wind vector. During the first 3 days following the eruption, the *1D_LOW_10* aerosol exhibits a more northward progression as indicated by the significant aerosol burden at 30°N in Figure 8e. The *1D_LOW_10* aerosol is advected northward by the prevailing southerly wind at ~45°E (Figure 8e), while the *1D_LOW_1* aerosol remains concentrated between 10°N and 20°N. The most dramatic difference in the [S]-weighted wind vector between *1D_LOW_1* and *1D_LOW_10* simulations occurs at day 7. Here *1D_LOW_1* indicates a continued progression westward in the easterly winds, while *1D_LOW_10* shows an almost complete reversal in the direction of advection owing to the influence of the anticyclone over Asia in this simulation. Figure 9 shows the 100 hPa wind vector superimposed on the 100 hPa wind speeds for *1D_LOW_1* and *1D_LOW_10*, evaluated 3 days after the eruption, and for ERA-interim reanalysis on 18 and 20 June 1991 [*Dee et al*., 2011]. It is clear that the northward advection of aerosol in *1D_LOW_10* is driven by the anticyclonic vortex centered over North India (30°N, 75°E) (Figure 9b), which is not present in *1D_LOW_1* at the equivalent time (Figure 9a). Although a similar southerly wind at ~45°E is present on 18 June in the reanalysis data (Figure 9c), it had dissipated by 20 June (Figure 9d). Anticyclogenesis over Asia in June is the result of warming over a region spanning Iraq to Tibet [*Yanai et al*., 1992], with anticyclonic anomalies then propagating eastward along the subtropical jet [*Watanabe and Yamazaki*, 2012] and eventually weakening by August [*Bourassa et al*., 2012]. *Bourassa et al*. [2012] suggested that an anticyclonic vortex over Asia was fundamental in the transport of the volcanic plume immediately after the 2011 Nabro (13°N, 41°E) eruption although these findings have been contested [*Fromm et al*., 2014]. What is clear is that the precise meteorological conditions that prevail during the eruption strongly influence the poleward progression of the aerosol. From Figures 8 and 9 we have shown that the aerosol transport out of the tropics is inextricably linked to the ambient wind direction, with the *1D_LOW_1* aerosol encountering a zonally dominant transport regime (Figure 8a). As a result, by day 30 the *1D_LOW_1* aerosol is primarily confined to the tropics (Figure 8d)

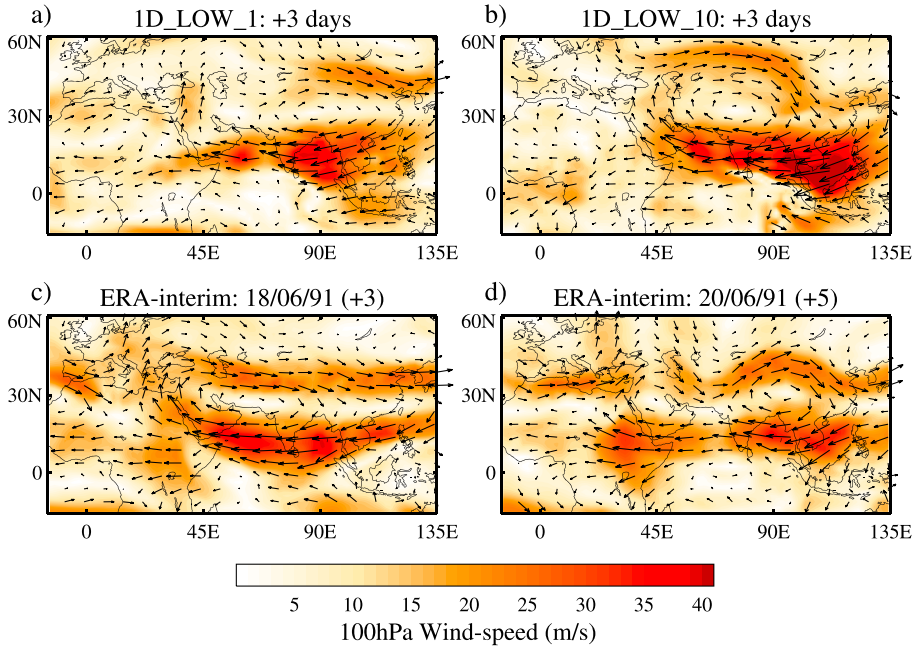

Figure 9. 100 hPa horizontal wind vector plotted on 100 hPa horizontal wind speed for (a) 1D_1 eruption + 3 days, (b) 1D_10 eruption + 3 days, (c) ERA-Interim 18 June 1991, and (d) ERA-Interim 20 June 1991 [*Dee et al.*, 2011].

at altitudes of ~40 hPa, while the *1D_LOW_10* aerosol is primarily confined to the NH (Figure 8h). Consequently, *1D_LOW_1* aerosol is transported into the SH within the upper branch of the BDC (Figure S8). By January 1992, 0.54 Tg [S] of combined SO_2 and SO_4 has been transported to the SH in *1D_LOW_1*, compared to 0.1 Tg [S] in *1D_LOW_10* (Figure S9).

3.4. Potential Climatic Consequences

The spatial distribution of the volcanic aerosol has important implications for the resultant climate impacts. *Haywood et al.* [2013] showed that hemispherically asymmetrical aerosol forcing is causally related to the displacement of the Intertropical Convergence Zone (ITCZ). For instance, the twentieth century NH volcanic eruptions of Novarupta-Katmai (June 1912) and El Chichón (March–April 1982) produced peak sulfate AOD hemispheric-asymmetries ($AOD_{NH\text{-}SH}$) of 0.08 and 0.07, respectively [*Sato et al.*, 1993; *Haywood et al.*, 2013], resulting in significant negative Sahelian precipitation anomalies in the subsequent year. In contrast, Pinatubo produced a peak $AOD_{NH\text{-}SH}$ of 0.04 and no significant shift in the ITCZ [*Haywood et al.*, 2013], although precipitation is generally suppressed subsequent to large volcanic eruptions owing to reductions in surface irradiances leading to reductions in latent heat fluxes and a slowing down of the hydrological cycle [*Trenberth and Dai*, 2007]. In these experiments, *1D_LOW_1* produces a peak $AOD_{NH\text{-}SH}$ of 0.05, which is close to the Pinatubo observations, while *1D_LOW_10* produces a peak $AOD_{NH\text{-}SH}$ of 0.10, which exceeds the observed $AOD_{NH\text{-}SH}$ for Novarupta-Katmai and El Chichón. Figure 10 shows the SW radiative flux anomalies at the tropopause for *1D_LOW_1* and *1D_LOW_10*, averaged over the two complete calendar years (January–December) following the eruption. The SW forcing is more spatially uniform for *1D_LOW_1* than for *1D_LOW_10*, which is a direct result of the location of the aerosol plume. For instance, the SW forcing in *1D_LOW_10* in the SH is negligible ($-0.25\ W/m^2$), while the SW forcing in the NH is significant ($-4.1\ W/m^2$). The standard deviation of the NH (30°N–90°N) mean net SW flux at the tropopause in the control simulation is 0.26; therefore, this SW forcing is significant at the 2σ level.

The aerosol burden in the tropical reservoir has implications for stratospheric dynamics and therefore stratospheric ozone concentrations [*Aquila et al.*, 2014]. Stratospheric sulfate aerosols provide surfaces for heterogeneous reactions between free radicals and ozone, which can result in ozone depletion [*Aquila et al.*, 2013]. Additionally, tropical stratospheric warming due to LW and near-infrared absorption within the aerosol layer would increase the local upwelling velocity and transport ozone-poor air in the lower stratosphere to higher

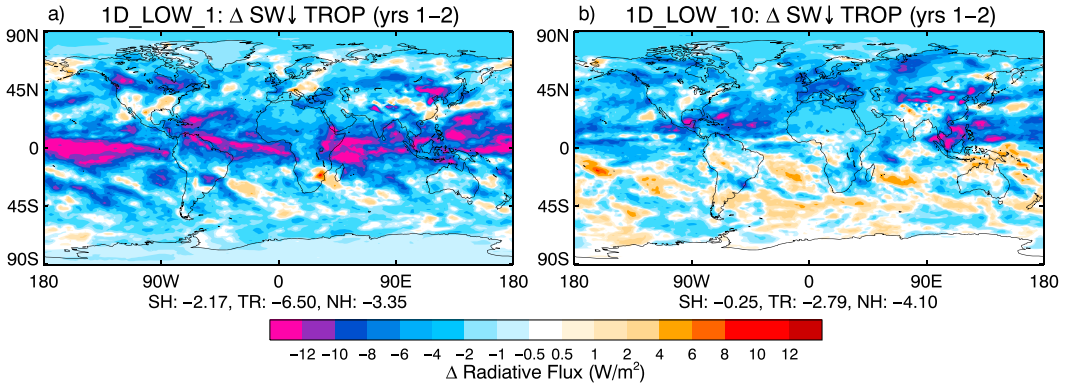

Figure 10. Tropopause short-wave net-downward radiation anomaly for 1D_LOW_1 and 1D_LOW_10 simulations averaged over two subsequent years following the eruption.

altitudes where ozone is more easily destroyed [*Schoeberl et al.*, 1993b]. Figure S10 shows the equatorial zonal mean wind perturbation for *1D_LOW_1*, *1D_LOW_10*, *1D_LOW_AV*, and *10D_LOW*. Tropical stratospheric aerosols promote a prolonged westerly QBO phase [*Aquila et al.*, 2014]. The greater tropical sulfate reservoir in *1D_LOW_1* causes a delay to the downward propagation of the easterly winds, which is exemplified by the positive (westerly) anomaly in *1D_LOW_1* at ~40 hPa following the eruption (Figure S10). *Labitzke* [1994] reports that after Pinatubo observations showed a warming of the lower stratosphere of about 3 K and a delay in the downward propagation of the easterly winds. Figure S11 shows the equatorial zonal mean zonal wind profiles for the Control and *1D_LOW_1* simulations. QBO phase changes are indicated in Figure S11 by the vertical black lines along 40 hPa altitude (where the QBO phase is defined by the zonal wind direction at 40 hPa) [*Baldwin et al.*, 2001]. From Figure S11, the first QBO phase change following Pinatubo is delayed by 1–2 months in the *1D_LOW_1* eruption compared to the control. Additionally, the significant aerosol concentration anomaly at the South Pole in November 1991 for *1D_LOW_1* (Figure 5c) would enhance heterogeneous ozone chemistry within the Antarctic vortex, as observed after the Pinatubo eruption [*McCormick et al.*, 1995].

4. Discussion

We have shown that the dispersion of volcanic aerosol can be highly sensitive to the ambient meteorology, with this sensitivity dependent on the altitude of SO_2 emission. While simulations using the 20 Tg [SO_2] *LOW* injection scenarios show a lot of sensitivity to meteorological conditions, simulations using the 14 Tg [SO_2] *HIGH* scenarios show little sensitivity. While it is difficult to determine whether the 20 Tg [SO_2] *LOW* or the 14 Tg [SO_2] HIGH simulations provide simulations that are more consistent with observations from global mean assessments of the AOD alone, assessment of the spatial distribution in both the horizontal and vertical suggests that, for our modeling study at least, members of the 20 Tg [SO_2] *LOW* ensemble are most consistent with observations. We find that the mean of the ten 1 day eruptions, where 20 Tg [SO_2] is emitted between 16 and 18 km altitude, provides a reasonable consistency with observations, but there is significant variability between the ensemble members. This variability is related to anomalous anticyclonic activity along the subtropical jet, which affects the "leakiness" of the tropical pipe and therefore the amount of aerosol that is retained within the tropical reservoir. We have discussed the implications of our results with respect to resultant climate changes, for instance, the possible effects of hemispherically asymmetric aerosol burdens on Sahelian precipitation, but note that a GCM with an interactive ocean model would be needed to comprehensively evaluate the climatic impacts of the different Pinatubo realizations. We have also compared the aerosol dispersion from a simulated 10 day eruption with the ensemble mean of the ten 1 day eruptions. These simulation designs represent two intuitive methods of overcoming the problem of variable meteorology. We have shown that the 10 day eruption is unable to produce the radiative heating and concomitant aerosol self-lofting required to transport aerosol to the SH; hence, the resultant spatial distribution of sulfate AOD compares inadequately to observations (Figure 3c). In contrast, the 1 day ensemble mean AOD anomaly is much closer to observations (Figure 3d); therefore, performing a 1 day eruption ensemble presents a better

solution to overcoming variable meteorology. However, the intraensemble variability in the *1D_LOW* experiments is significant; for instance, *1D_LOW_9* and *1D_LOW_10* fail to capture the SH transport of aerosol observed after Pinatubo (Figures 7i and 7j). Assuming that the *1D_LOW* results represent the complete set of possible realizations of the Pinatubo eruption, this would mean a 20% chance of obtaining a "failed" simulation for the specific goal of obtaining SH transport.

We have also performed simulations in which 20 Tg [SO_2] is emitted within a 3 h span between 16 and 18 km altitude (*3H_LOW*). The 3 h duration was selected to represent the cataclysmic Pinatubo eruption that occurred on 15 June 1991 [*Holasek et al*., 1996]. We find that our results from a 24 h period are equivalent to those from a 3 h eruption. However, we qualify this result by noting the limitations of the aerosol microphysics scheme employed here, which only consists of two sulfate size modes. Additionally, SO_2 is not the only substance emitted by volcanic eruptions—volcanic ash is co-emitted and would very likely change the heating rates due to the predominance of coarse mode aerosols [e.g., *Niemeier et al*., 2009] that are effective absorbers of infrared radiation. We have also performed simulations in which the Cerro Hudson eruption that occurred on 15 August 1991 is represented by a 3.3 Tg [SO_2] injection between 11 and 15 km altitude at (46°S, 73°W), in an eruption that lasts 8 h. We find little difference in zonal mean AOD between simulations with and without the Cerro Hudson eruption (Figure S7).

Our results are conditional on the selected specifications of the eruption and the specifications of HadGEM2-CCS. For instance, we have shown that the aerosol dispersion after a high-altitude SO_2 emission scenario (19–29 km) is substantially less sensitive to the existing meteorological state, which is due to the limited meteorological variability in the middle stratosphere. It is therefore imperative to precisely identify the initial location of the volcanic plume in order to accurately model the concomitant aerosol transport. An eruption during a different month might also avoid the variability associated with the Asian anticyclone, which is a seasonal (June–August) phenomenon [*Park et al*., 2007], and an eruption during a different QBO phase would alter the permeability of the tropical pipe [*Trepte et al*., 1993]. Additionally, the representation of sulfate aerosol in HadGEM2-CCS is limited to two hygroscopic modes with fixed dry-mode radii [*Bellouin et al*., 2007]. Observations from the post-Pinatubo era showed that the global sulfate size distribution continued to grow for 1.5 years after the eruption to attain effective radii of approximately 0.6–0.8 μm [*Stenchikov et al*., 1998; *Russell et al*., 1996], whereas the accumulation-mode aerosol in these simulations is fixed at a geometric mean radius of a lognormal mode of 0.376 μm. Larger particles experience greater fall velocities [*Rasch et al*., 2008] and absorb more efficiently in the LW and near-infrared spectrum and scatter less efficiently in the SW spectrum. Our model might therefore underestimate the gravitational sedimentation rates and LW heating rates exhibited by the volcanic aerosol. Inevitably, the sea surface temperature and meteorological state in our simulations are unrelated to the observed post-Pinatubo conditions. Our simulations therefore include a subset of possible meteorological conditions that could be encountered by a volcanic-aerosol plume, conditions which would also differ with season and latitude of eruption. For interest, the ongoing model intercomparison project VolMIP (http://volmip.org/experiments.html) also selected to use preindustrial baseline conditions for their eruption simulations. VolMIP's VolLongS60EQ scenario is comparable in design to our simulations (but with a significantly greater SO_2 emission of 100 Tg); therefore a direct evaluation of the aerosol plume evolution in that scenario could prove elucidative. One final caveat is that we prescribed ozone concentrations for the duration of these simulations; therefore, the model excludes simulation of the ozone changes from heterogeneous reactions on the aerosol surfaces (and the resultant feedback) such as observed after Pinatubo [*McCormick et al*., 1995]. We believe that these caveats, however, do not alter the primary result of this research: that volcanic aerosol plume evolution can be highly sensitive to the existing meteorological state.

With the improved representation of stratospheric aerosol in climate models, it is tempting to suggest that the models might disregard the imposition of climatologies of stratospheric aerosol concentrations in favor of simply injecting SO_2 and relying on the aerosol scheme to provide sulfate aerosol concentrations that are self-consistent with the meteorology. However, the extreme variability evidenced by the factor of 2 difference between the AOD in the *1D_LOW_1* and *1D_LOW_10* scenarios (Figure 2) suggests that the meteorological variability may compromise results: studies may "get lucky" and represent a particular volcanic eruption with reasonable fidelity, but they may not. Indeed, the chances of successfully representing all significant volcanic eruptions in the twentieth century (Novarupta-Katmai, Agung (March, May 1963), El Chichón, and Pinatubo) can be estimated from our statistics as around 0.8^4 or ~0.4, indicating that the chances of simulating all

volcanoes with reasonable fidelity is less than 50:50. Our results also suggest that simply averaging by simulating a multiple-day eruption cannot represent the heating rates in the atmosphere and hence correctly model aerosol-dispersion. Our study suggests that centennial scale modeling such as the CMIP6 "deck" may wish to stick to tried and tested climatological stratospheric aerosol concentrations. Our study also suggests that future climate model simulations should account for meteorological variability when simulating volcanic eruptions.

Author Contribution

ACJ designed and performed the simulations and wrote the paper with assistance from all co-authors. Additionally, AJ provided the model configuration and VA provided the SAGE II/AVHRR data and supporting information.

Acknowledgments

A.C.J. was funded by a NERC/CASE PhD studentship (ref. 580 009 138, with CASE partner being the Met Office); J.M.H. and A.J. were supported by the Joint UK DECC/Defra Met Office Hadley Centre Climate Programme (GA01101). The authors would like to thank Larry Thomason for supplying the SAGE II data. Data are freely available by contacting A.C.J. (anthony.jones@metoffice.gov.uk)

References

Aquila, V., L. D. Oman, R. S. Stolarski, P. R. Colarco, and P. A. Newman (2012), Dispersion of the volcanic sulfate cloud from a Mount Pinatubo-like eruption, *J. Geophys. Res.*, *117*, D06216, doi:10.1029/2011JD016968.

Aquila, V., L. D. Oman, R. Stolarski, A. R. Douglass, and P. A. Newman (2013), The response of ozone and nitrogen dioxide to the eruption of Mt. Pinatubo at southern and northern midlatitudes, *J. Atmos. Sci.*, *70* (3), 894–900, doi:10.1175/JAS-D-12-0143.1.

Aquila, V., C. I. Garfinkel, P. A. Newman, L. D. Oman, and D. W. Waugh (2014), Modifications of the quasi-biennial oscillation by a geoengineering perturbation of the stratospheric aerosol layer, *Geophys. Res. Lett.*, *41*, 1738–1744, doi:10.1002/2013GL058818.

Arfeuille, F., B. P. Luo, P. Heckendorn, D. Weisenstein, J. X. Sheng, E. Rozanov, M. Schraner, S. Brönnimann, L. W. Thomason, and T. Peter (2013), Modeling the stratospheric warming following the Mt. Pinatubo eruption: uncertainties in aerosol extinctions, *Atmos. Chem. Phys.*, *13*(22), 11,221–11,234, doi:10.5194/acp-13-11221-2013.

Baldwin, M. P., et al. (2001), The quasi-biennial oscillation, *Rev. Geophys.*, *39*(2), 179–229, doi:10.1029/1999RG000073.

Bellouin, N., O. Boucher, J. Haywood, C. Johnson, A. Jones, J. Rae, and S. Woodward (2007), Improved representation of aerosols for HadGEM2, Tech. Note 73, Hadley Centre, Met Office, Exeter, U. K., 42 pp. [Available at http://www.metoffice.gov.uk/media/pdf/8/f/HCTN_73.pdf (last accessed 01/16).]

Bellouin, N., J. Rae, A. Jones, C. Johnson, J. Haywood, and O. Boucher (2011), Aerosol forcing in the Climate Model Intercomparison Project (CMIP5) simulations by HadGEM2-ES and the role of ammonium nitrate, *J. Geophys. Res.*, *116*, D20206, doi:10.1029/2011JD016074.

Bluth, G. J. S., S. D. Doiron, C. C. Schnetzler, A. J. Krueger, and L. S. Walker (1992), Global tracking of the SO2 clouds from the June, 1991 Mount Pinatubo eruptions, *Geophys. Res. Lett.*, *19*(2), 151–154, doi:10.1029/91GL02792.

Bourassa, A. E., A. Robock, W. J. Randel, T. Deshler, L. A. Rieger, N. D. Lloyd, E. J. Llewellyn, and D. A. Degenstein (2012), Large volcanic aerosol load in the stratosphere linked to Asian monsoon transport, *Science*, *337*(6090), 78–81, doi:10.1126/science.1219371.

Boville, B. A., J. R. Holton, and P. W. Mote (1991), Simulation of the Pinatubo aerosol cloud in general circulation model, *Geophys. Res. Lett.*, *18*(12), 2281–2284, doi:10.1029/91GL02778.

Choi, W., W. B. Grant, J. H. Park, K.-M. Lee, H. Lee, and J. M. Russell III (1998), Role of the quasi-biennial oscillation in the transport of aerosols from the tropical stratospheric reservoir to midlatitudes, *J. Geophys. Res.*, *103*, 6033–6042, doi:10.1029/97JD03118.

Cionni, I., V. Eyring, J. F. Lamarque, W. J. Randel, D. S. Stevenson, F. Wu, G. E. Bodeker, T. G. Shepherd, D. T. Shindell, and D. W. Waugh (2011), Ozone database in support of CMIP5 simulations: Results and corresponding radiative forcing, *Atmos. Chem. Phys.*, *11*, 11,267–11,292, doi:10.5194/acp-11-11267-2011.

Dee, D. P., et al. (2011), The ERA-Interim reanalysis: Configuration and performance of the data assimilation system, *Q. J. R. Meteorol. Soc.*, *137*, 553–597, doi:10.1002/qj.828.

Deshler, T., and R. Anderson-Sprecher (2006), Non-volcanic stratospheric aerosol trends: 1971–2004, in *Assessment of Stratospheric Aerosol Properties*, edited by L. Thomason and T. Peter WCRP 124, WMO/TD 1295, SPARC Rep. 4, chap. 5, pp. 177–218, World Meteorol. Organ., Geneva, Switz.

Dhomse, S. S., et al. (2014), Aerosol microphysics simulations of the Mt. Pinatubo eruption with the UM-UKCA composition-climate model, *Atmos. Chem. Phys.*, *14*, 11,221–11,246, doi:10.5194/acp-14-11221-2014.

Driscoll, S., A. Bozzo, L. J. Gray, A. Robock, and G. Stenchikov (2012), Coupled Model Intercomparison Project 5 (CMIP5) simulations of climate following volcanic eruptions, *J. Geophys. Res.*, *117*, D17105, doi:10.1029/2012JD017607.

Edwards, J. M., and A. Slingo (1996), Studies with a flexible new radiation code. I: Choosing a configuration for a large-scale model, *Q. J. R. Meteorol. Soc.*, *122*, 689–719.

English, J. M., O. B. Toon, and M. J. Mills (2013), Microphysical simulations of large volcanic eruptions: Pinatubo and Toba, *J. Geophys. Res. Atmos.*, *118*, 1880–1895, doi:10.1002/jgrd.50196.

Fromm, M., G. Kablick III, G. Nedoluha, E. Carboni, R. Grainger, J. Campbell, and J. Lewis (2014), Correcting the record of volcanic stratospheric aerosol impact: Nabro and Sarychev Peak, *J. Geophys. Res. Atmos.*, *119*, 10,343–10,364, doi:10.1002/2014JD021507.

Gray, L. J., A. A. Scaife, D. M. Mitchell, S. Osprey, S. Ineson, S. Hardiman, N. Butchart, J. Knight, R. Sutton, and K. Kodera (2013), A lagged response to the 11 year solar cycle in observed winter Atlantic/European weather patterns, *J. Geophys. Res. Atmos.*, *118*, 13,405–13,420, doi:10.1002/2013JD020062.

Guo, S., G. S. Bluth, W. I. Rose, I. M. Watson, and A. J. Prata (2004), Re-evaluation of the SO2 release of the 15 June 1991 Pinatubo eruption using ultraviolet and infrared satellite sensors, *Geochem. Geophys. Geosyst.*, *5*, Q04001, doi:10.1029/2003GC000654.

Hansen, J., A. Lacis, R. Reudy, and M. Sato (1992), Potential climate impact of Mount Pinatubo eruption, *Geophys. Res. Lett.*, *19*(2), 215–218, doi:10.1029/91GL02788.

Hardiman, S. C., N. Butchart, T. J. Hinton, S. M. Osprey, and L. J. Gray (2012), The effect of a well-resolved stratosphere on surface climate: Differences between CMIP5 simulations with high and low top versions of the Met Office climate model, *J. Clim.*, *25*, 7083–7099, doi:10.1175/JCLI-D-11-00579.1.

Haywood, J. M., et al. (2010), Observations of the eruption of the Sarychev volcano and simulations using the HadGEM2 climate model, *J. Geophys. Res.*, *115*, D21212, doi:10.1029/2010JD014447.

Haywood, J. M., A. Jones, N. Bellouin, and D. Stephenson (2013), Asymmetric forcing from stratospheric aerosol impacts Sahelian rainfall, *Nat. Clim. Change*, *3*, 660–665, doi:10.1038/nclimate1857.

Hofmann, D. J., S. J. Oltmans, J. M. Harris, S. Solomon, T. Deshler, and B. J. Johnson (1992), Observation and possible causes of new ozone depletion in Antarctica in 1991, *Nature*, *359*, 283–287, doi:10.1038/359283a0.

Holasek, R. E., S. Self, and A. W. Woods (1996), Satellite observations and interpretation of the 1991 Mount Pinatubo eruption plumes, *J. Geophys. Res.*, *101*(B12), 27,635–27,655, doi:10.1029/96JB01179.

Holton, J. R., P. H. Haynes, M. E. McIntyre, A. R. Douglass, R. B. Rood, and L. Pfister (1995), Stratosphere-troposphere exchange, *Rev. Geophys.*, *33*(4), 403–439, doi:10.1029/95RG02097.

Jackson, L. S., J. A. Crook, A. Jarvis, D. Leedal, A. Ridgwell, N. Vaughan, and P. M. Forster (2015), Assessing the controllability of Arctic sea ice extent by sulfate aerosol geoengineering, *Geophys. Res. Lett.*, *42*, 1223–1231, doi:10.1002/2014GL062240.

Jones, A. C., J. M. Haywood, and A. Jones (2016), Climatic impacts of stratospheric geoengineering with sulfate, black carbon and titania injection, *Atmos. Chem. Phys.*, *16*(5), 2843–2862, doi:10.5194/acp-16-2843-2016.

Jones, C. D., et al. (2011), The HadGEM2-ES implementation of CMIP5 centennial simulations, *Geosci. Model Dev.*, *4*, 543–570, doi:10.5194/gmd-4-543-2011.

Kirchner, I., G. L. Stenchikov, H.-F. Graf, A. Robock, and J. C. Antuña (1999), Climate model simulation of winter warming and summer cooling following the 1991 Mount Pinatubo volcanic eruption, *J. Geophys. Res.*, *104*(D16), 19,039–19,055, doi:10.1029/1999JD900213.

Labitzke, K. (1994), Stratospheric temperature changes after the Pinatubo eruption, *J. Atmos. Terr. Phys.*, *56*(9), 1027–1034, doi:10.1016/0021-9169(94)90039-6.

Labitzke, K., and M. P. McCormick (1992), Stratospheric temperature increases due to Pinatubo aerosols, *Geophys. Res. Lett.*, *19*(2), 207–210, doi:10.1029/91GL02940.

Legates, D. R., and G. J. McCabe Jr. (1999), Evaluating the use of "goodness-of-fit" measures in hydrologic and hydroclimatic model validation, *Water Resour. Res.*, *35*(1), 233–241, doi:10.1029/1998WR900018.

Legrand, M., and D. Wagenbach (1999), Impact of the Cerro Hudson and Pinatubo volcanic eruptions on the Antarctic air and snow chemistry, *J. Geophys. Res.*, *104*(D1), 1581–1596, doi:10.1029/1998JD100032.

Martin, G. M., M. A. Ringer, V. D. Pope, A. Jones, C. Dearden, and T. J. Hinton (2006), The physical properties of the atmosphere in the new Hadley Centre Global Environmental Model, HadGEM1. Part 1: Model description and global climatology, *J. Clim.*, *19*(7), 1274–1301, doi:10.1175/JCLI3636.1.

Martin, G. M., et al. (2011), The HadGEM2 family of Met Office Unified Model climate configurations, *Geosci. Model Dev.*, *4*, 723–757, doi:10.5194/gmd-4-723-2011.

McCormick, M. P., and R. E. Veiga (1992), SAGE II measurements of early Pinatubo aerosols, *Geophys. Res. Lett.*, *19*(2), 155–158, doi:10.1029/91GL02790.

McCormick, M. P., L. W. Thomason, and C. R. Trepte (1995), Atmospheric effects of the Mt Pinatubo eruption, *Nature*, *373*, 399–404, doi:10.1038/373399a0.

Mills, M. J., et al. (2016), Global volcanic aerosol properties derived from emissions, 1990–2014, using CESM1(WACCM), *J. Geophys. Res. Atmos.*, *121*, 2332–2348, doi:10.1002/2015JD024290.

Mitchell, D. M., S. M. Osprey, L. J. Gray, N. Butchart, S. C. Hardiman, A. J. Charlton-Perez, and P. Watson (2012), The effect of climate change on the variability of the Northern Hemisphere stratospheric polar vortex, *J. Atmos. Sci.*, *69*, 2609–2618, doi:10.1175/JAS-D-12-021.1.

Niemeier, U., C. Timmreck, H.-F. Graf, S. Kinne, S. Rast, and S. Self (2009), Initial fate of fine ash and sulfur from large volcanic eruptions, *Atmos. Chem. Phys.*, *9*, 9043–9057, doi:10.5194/acp-9-9043-2009.

Oman, L., A. Robock, G. Stenchikov, T. Thordarson, D. Koch, D. Shindell, and C. Gao (2006), Modeling the distribution of the volcanic aerosol cloud from the 1783 Laki Eruption, *J. Geophys. Res.*, *111*, D12209, doi:10.1029/2005JD006899.

Park, M., W. J. Randel, A. Gettelman, S. T. Massie, and J. H. Jiang (2007), Transport above the Asian summer monsoon anticyclone inferred from Aura Microwave Limb Sounder tracers, *J. Geophys. Res.*, *112*, D16309, doi:10.1029/2006JD008294.

Pudykiewicz, J. A., and A. P. Dastoor (1995), On numerical simulation of the global distribution of sulfate aerosol produced by a large volcanic eruption, *J. Clim.*, *8*, 464–473, doi:10.1175/1520-0442(1995)008<0464:ONSOTG>2.0.CO;2.

Rasch, P. J., P. J. Crutzen, and D. B. Coleman (2008), Exploring the geoengineering of climate using stratospheric sulfate aerosols: The role of particle size, *Geophys. Res. Lett.*, *35*, L02809, doi:10.1029/2007GL032179.

Read, W. G., L. Froidevaux, and J. W. Waters (1993), Microwave Limb Sounder measurement of stratospheric SO2 from the Mt. Pinatubo volcano, *Geophys. Res. Lett.*, *20*(12), 1299–1302, doi:10.1029/93GL00831.

Robock, A. (2000), Volcanic eruptions and climate, *Rev. Geophys.*, *38*(2), 191–219, doi:10.1029/1998RG000054.

Robock, A., and J. Mao (1995), The volcanic signal in surface temperature observations, *J. Clim.*, *8*, 1086–1103.

Russell, P. B., et al. (1996), Global to microscale evolution of the Pinatubo volcanic aerosol derived from diverse measurements and analyses, *J. Geophys. Res.*, *101*(D13), 18,745–18,763, doi:10.1029/96JD01162.

Sato, M., J. E. Hansen, M. P. McCormick, and J. B. Pollack (1993), Stratospheric aerosol optical depth, 1850–1990, *J. Geophys. Res.*, *98*, 22,987–22,994, doi:10.1029/93JD02553.

Schoeberl, M. R., S. D. Doiron, L. R. Lait, P. A. Newman, and A. J. Krueger (1993a), A simulation of the Cerro Hudson SO_2 cloud, *J. Geophys. Res.*, *98*(D2), 2949–2955, doi:10.1029/92JD02517.

Schoeberl, M. R., P. K. Bhartia, and E. Hilsenrath (1993b), Tropical ozone loss following the eruption of Mt. Pinatubo, *Geophys. Res. Lett.*, *20*(1), 29–32, doi:10.1029/92GL02637.

Self, S., R. Gertisser, T. Thordarson, M. R. Rampino, and J. A. Wolff (2004), Magma volume, volatile emissions, and stratospheric aerosols from the 1815 eruption of Tambora, *Geophys. Res. Lett.*, *31*, L20608, doi:10.1029/2004GL020925.

Sheng, J.-X., D. K. Weisenstein, B.-P. Luo, E. Rozanov, F. Arfeuille, and T. Peter (2015), A perturbed parameter model ensemble to investigate Mt. Pinatubo's 1991 initial sulfur mass emission, *Atmos. Chem. Phys.*, *15*, 11,501–11,512, doi:10.5194/acp-15-11501-2015.

Soden, B. J., R. T. Wetherald, G. L. Stenchikov, and A. Robock (2002), Global cooling after the eruptions of Mount Pinatubo: A test of climate feedback by water vapor, *Science*, *296*(5568), 727–730, doi:10.1126/science.296.5568.727.

Spencer, R. W., F. J. LaFontaine, T. DeFelice, and F. J. Wentz (1998), Tropical oceanic precipitation changes after the 1991 Pinatubo eruption, *J. Atmos. Sci.*, *55*, 1707–1713, doi:10.1175/1520-0469(1998)055<1707:TOPCAT>2.0.CO;2.

Stenchikov, G. L., I. Kirchner, A. Robock, H.-F. Graf, J. C. Antuña, R. G. Grainger, A. Lambert, and L. Thomason (1998), Radiative forcing from the 1991 Mount Pinatubo volcanic eruption, *J. Geophys. Res.*, *103*(D12), 13,837–13,857, doi:10.1029/98JD00693.

Stowe, L. L., R. M. Carey, and P. P. Pellegriao (1992), Monitoring the Mt. Pinatubo aerosol layer with NOAA/11 AVHRR data, *Geophys. Res. Lett.*, *19*(2), 159–162, doi:10.1029/91GL02958.

Taylor, K. E., R. J. Stouffer, and G. A. Meehl (2012), An overview of CMIP5 and the experiment design, *Bull. Am. Meteorol. Soc.*, *93*, 485–498, doi:10.1175/BAMS-D-11-00094.1.

Timmreck, C., H. Graf, and I. Kirchner (1999a), A one and half year interactive MA/ECHAM4 simulation of Mount Pinatubo aerosol, *J. Geophys. Res.*, *104*(D8), 9337–9359, doi:10.1029/1999JD900088.

Timmreck, C., H. Graf, and J. Feichter (1999b), Simulation of Mt. Pinatubo volcanic aerosol with the Hamburg climate model ECHAM4, *Theor. Appl. Climatol.*, *62*(3–4), 85–108, doi:10.1007/s007040050076.

Toohey, M., K. Krüger, U. Niemeier, and C. Timmreck (2011), The influence of eruption season on the global aerosol evolution and radiative impact of tropical volcanic eruptions, *Atmos. Chem. Phys.*, *11*, 12,351–12,367, doi:10.5194/acp-11-12351-2011.

Trenberth, K. E., and A. Dai (2007), Effects of the Mount Pinatubo volcanic eruption on the hydrological cycle as an analog of geoengineering, *Geophys. Res. Lett.*, *34*, L15702, doi:10.1029/2007GL030524.

Trepte, C. R., and M. H. Hitchman (1992), Tropical stratospheric circulation deduced from satellite aerosol data, *Nature*, *355*, 626–628, doi:10.1038/355626a0.

Trepte, C. R., R. E. Veiga, and M. P. McCormick (1993), The poleward dispersal of Mount Pinatubo volcanic aerosol, *J. Geophys. Res.*, *98*(D10), 18, 563–18, 573, doi:10.1029/93JD01362.

Watanabe, T., and K. Yamazaki (2012), Influence of the anticyclonic anomaly in the subtropical jet over the Western Tibetan Plateau on the intraseasonal variability of the summer Asian monsoon in early summer, *J. Clim.*, *25*, 1291–1303, doi:10.1175/JCLI-D-11-00036.1.

Watson, P. A. G., and L. J. Gray (2014), The stratospheric wintertime response to applied extratropical torques and its relationship with the annular mode, *Clim. Dyn.*, *44*, 2513–2537, doi:10.1007/s00382-014-2359-2.

Weisenstein, D. K., J. E. Penner, M. Herzog, and X. Liu (2007), Global 2-D intercomparison of sectional and modal aerosol modules, *Atmos. Chem. Phys.*, *7*, 2339–2355, doi:10.5194/acp-7-2339-2007.

Yanai, M., C. Li, and Z. Song (1992), Seasonal heating of the Tibetan Plateau and its effects on the evolution of the Asian summer monsoon, *J. Meteorol. Soc. Jpn.*, *70*, 319–351.

Young, R. E., H. Houben, and O. B. Toon (1994), Radiatively forced dispersion of the Mt. Pinatubo volcanic cloud and induced temperature perturbations in the stratosphere during the first few months following the eruption, *Geophys. Res. Lett.*, *21*(5), 369–372, doi:10.1029/93GL03302.

Zhao, T. X.-P., P. K. Chan, and A. K. Heidinger (2013), A global survey of the effect of cloud contamination on the aerosol optical thickness and its long-term trend derived from operational AVHRR satellite observations, *J. Geophys. Res. Atmos.*, *118*, 2849–2857, doi:10.1002/jgrd.50278.